Missouri University of Science and Technology
Scholars' Mine

Mechanical and Aerospace Engineering Faculty Research & Creative Works

Mechanical and Aerospace Engineering

01 Jul 2020

Effects of Zirconia Doping on Additively Manufactured Alumina Ceramics by Laser Direct Deposition

John M. Pappas

Aditya R. Thakur

Xiangyang Dong
Missouri University of Science and Technology, dongxi@mst.edu

Follow this and additional works at: https://scholarsmine.mst.edu/mec_aereng_facwork

 Part of the Mechanical Engineering Commons

Recommended Citation

J. M. Pappas et al., "Effects of Zirconia Doping on Additively Manufactured Alumina Ceramics by Laser Direct Deposition," *Materials and Design*, vol. 192, Elsevier Ltd, Jul 2020.
The definitive version is available at https://doi.org/10.1016/j.matdes.2020.108711

This work is licensed under a Creative Commons Attribution-Noncommercial-No Derivative Works 4.0 License.

This Article - Journal is brought to you for free and open access by Scholars' Mine. It has been accepted for inclusion in Mechanical and Aerospace Engineering Faculty Research & Creative Works by an authorized administrator of Scholars' Mine. This work is protected by U. S. Copyright Law. Unauthorized use including reproduction for redistribution requires the permission of the copyright holder. For more information, please contact scholarsmine@mst.edu.

Materials and Design 192 (2020) 108711

Contents lists available at ScienceDirect

Materials and Design

journal homepage: www.elsevier.com/locate/matdes

Effects of zirconia doping on additively manufactured alumina ceramics by laser direct deposition

John M. Pappas, Aditya R. Thakur, Xiangyang Dong *

Mechanical and Aerospace Engineering, Missouri University of Science and Technology, Rolla, MO 65409, USA

HIGHLIGHTS

- Zirconia doping greatly reduced crack length during laser direct deposition of alumina ceramics.
- Doping helped substantially reduce grain size and critical flaw size within printed ceramics.
- Deposited ceramics were toughened due to crack interaction with zirconia doped grain boundary.
- Design by doping was an efficient way in tailoring properties of laser direct deposited ceramics.

GRAPHICAL ABSTRACT

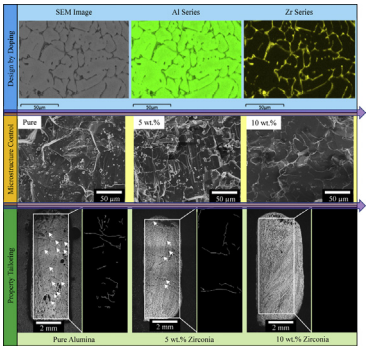

ARTICLE INFO

Article history:
Received 13 January 2020
Received in revised form 31 March 2020
Accepted 1 April 2020
Available online 27 April 2020

Keywords:
Laser direct deposition
Alumina ceramics
Additive manufacturing
Microstructure
Mechanical properties

ABSTRACT

The ability to additively manufacture functional alumina ceramics has the potential to lower manufacturing costs and development time for complex components. In this study, the doping effects of zirconia on laser direct deposited alumina ceramics were investigated. The microstructure of the printed samples was analyzed in terms of grain size and composition distribution. The addition of zirconia was found to accumulate along alumina grain boundaries and resulted in significant grain refinement. The zirconia doping largely reduced crack formation during processing compared to that of pure alumina samples. In the case of 10 wt% zirconia, cracking during deposition was nearly completely eliminated, but meanwhile porosity was increased. Through grain refinement and crack reduction in 10 wt% zirconia samples, bending strength was shown to increase by nearly four times the value obtained with pure alumina. Fracture toughness was also shown to increase by 1.5 times with addition of 5 wt% zirconia, which was attributed to the crack interaction with zirconia doped grain boundary and stress induced tetragonal to monoclinic transformation of zirconia. These findings indicated the potentials of dopants during laser direct deposition of ceramics and can further be used to tailor the properties of additively manufactured ceramic components.

© 2018 The Authors. Published by Elsevier Ltd. This is an open access article under the CC BY-NC-ND license (http://creativecommons.org/licenses/by-nc-nd/4.0/).

1. Introduction

Alumina ceramics are widely used in industry owing to many desirable qualities including excellent compressive strength, electrical and thermal insulation, wear and chemical resistance, and relatively low density. Excellent mechanical properties of high-purity alumina along

* Corresponding author.
E-mail address: dongxi@mst.edu (X. Dong).

https://doi.org/10.1016/j.matdes.2020.108711
0264-1275/© 2018 The Authors. Published by Elsevier Ltd. This is an open access article under the CC BY-NC-ND license (http://creativecommons.org/licenses/by-nc-nd/4.0/).

with biocompatibility also make alumina ceramics a viable option for dental and medical applications including orthopedic and dental reparation [1]. Although alumina ceramics exhibit high hardness, strength, and elastic modulus, relatively low fracture toughness hinders the application of laser-based additive manufacturing in these materials.

A typical ceramic toughening mechanism includes crack bridging, branching, pinning, and deflection as reported previously [2]. Also, an important method to increase fracture strength and toughness of as-fabricated ceramics is through addition of a secondary phase like zirconia [3]. For traditionally sintered alumina, it was found that small amounts of added zirconia resulted in microstructural refinement [4] and improved mechanical properties of produced ceramics. In addition to grain refinement, addition of partially stabilized zirconia has a stress-induced transformation to monoclinic crystal structure resulting in a volume expansion of 3–5%, which improves fracture toughness for alumina-zirconia composites [5]. Naglieri et al. [6] found that microstructural features of alumina-zirconia composites, fabricated by pressureless sintering, could be tailored by varying zirconia content from 5 to 20 vol%. Wu et al. [7] studied the effects of TiO_2 doping on the mechanical properties and microstructure of laser direct deposited alumina/aluminum titanate composites. In their study, it was found that dopant percentages between 2 and 6 mol% were best for mechanical properties including flexural strength, fracture toughness, and microhardness. Wilkes et al. [8] found that by using a mixture of alumina and zirconia at the eutectic ratio, fine grained eutectic composite microstructures were achieved using selective laser melting. With high preheating temperatures at 1600 °C, near fully dense, crack-free ceramics were fabricated. Due to the fine-grained microstructure and limited defects, flexural strength was comparable to the reported values for ceramics of similar composition fabricated by conventional methods. Adding zirconia to alumina ceramics was also shown to be an effective way of controlling the microstructure in ceramics and toughening printed samples through crack bridging and deflection [2]. Li et al. [9] studied microstructural characteristics of Al_2O_3-ZrO_2 ceramics printed with laser direct deposition with zirconia content >35 wt%. However, previous studies on laser-based additive manufacturing of alumina ceramics focused on either pure [10,11], 10 wt% zirconia [2] or the eutectic ratio [8,12,13]. Very few studies have been performed to directly compare the effects of varying zirconia percentages on resultant ceramic microstructure, crack formation, and mechanical properties including microhardness, mechanical strength, and fracture toughness. Varying zirconia percentages may result in different toughening mechanisms, where increased monoclinic phase at higher zirconia contents [6] would hinder stress induced phase transformation. A optimal doping percentage thus may exist in order to achieve highest fracture toughness and flexural strength [7,14] during laser direct deposition.

Cracks observed in laser deposited ceramics are typically caused by high thermal gradients and resultant stresses. Fan et al. [15] found that micro-cracking in yttria stabilized zirconia ceramics can be significantly reduced by careful selection of laser power, with an optimal laser power between 300 and 325 W found for thin wall structures fabricated by laser engineered net shaping. Wilkes et al. [8] found that by preheating each layer with a secondary CO_2 laser beam prior to deposition, microcracking could also be eliminated in selective laser melting of alumina-zirconia ceramics. Again, while extensive studies were reported on the effects of processing conditions, very few studies investigated the effects of compositions on the crack formation.

This study proposes to directly compare the microstructural characteristics and mechanical properties, in particular crack formation, of alumina ceramics produced with varied zirconia doping compositions. Thin wall and cylindrical structures were fabricated with zirconia doping content ranging from 0 to 10 wt%. The effects of zirconia content on microstructure including cracking, porosity, and grain size were examined. Printed samples were also characterized for mechanical properties including microhardness, fracture toughness, and flexural strength at each zirconia doping percentage. A detailed investigation of doped zirconia distribution within the printed samples provided insights in designing additively manufactured ceramics via doping, showing the potentials of further tailoring ceramic microstructure and mechanical properties by laser direct deposition. For example, if the ceramic parts will be used in an application where it may see a substantial bending load, a zirconia composition near 10 wt% showed potentials of the highest bending strength due to reduced critical flaw size within the nearly crack-free samples. In critical applications where fracture toughness needs to be maximized [16], a zirconia content of approximately 5 wt% proved to be best for the tetragonal to monoclinic toughening mechanism of the zirconia phase. An example application for using this process is to additively manufacture zirconia toughened alumina crowns and dental implants with zirconia dopant percentage between 5 and 10 wt%, where flexural strength and toughness are of high importance [16]. Finally, laser direct deposited pure alumina is best for applications where high hardness is of interest, such as wear resistant coatings deposited onto dissimilar materials [17]. Most importantly, this study clearly demonstrated that zirconia doping substantially reduced cracks developed during deposition. A combination of fewer cracks and reduced grain size results in bending strength nearly four times greater than that measured for pure alumina.

2. Experimental procedure

2.1. Materials

Commercially pure (>99.7%) alumina powder (A3500 UG, Almatis) with a D50 particle size of 2.2 μm was used in this study. Yttria partially stabilized zirconia (TZ-3Y-E, TOSOH) was used as an additive at 5 wt% and 10 wt% in pure alumina powders to prepare thin wall and cylindrical structures in this study. Alumina (99.8%) (AD998, CoorsTek) was used as substrates due to its thermal expansion compatibility with the deposited materials. Alumina and zirconia powders were mixed in a ball mill for 2 h using alumina grinding media and acetone solvent. Acetone solvent was removed with a Buchi R124 rotary evaporator. Following rotary evaporation, the powder was calcined for 6 h in a Lindberg furnace at 600 °C to remove any residual moisture or acetone. Large powder agglomerates were removed by sieving powder mixtures through a 325-mesh sieve prior to fabrication.

2.2. Experimental setup

A schematic of the experimental setup used in this study is shown in Fig. 1. The laser direct deposition setup included a 1.7 kW computer-controlled CO_2 laser (Convergent Energy Ultimate Model) with a wavelength of 10.6 μm and Gaussian beam intensity profile. A 3-axis computer numerically controlled (CNC) motorized table was utilized for positioning and movement control. The laser beam was focused with a 127 mm focal length ZnSe lens to give a stable beam with 2.5 mm spot size. Fig. 2 shows the laser direct deposition process in fabricating ceramic components. Fig. 2A and Fig. 2B demonstrate the printing processes for thin wall structures and cylindrical structures, respectively. The typical obtained parts are highlighted in Fig. 2C and D, respectively.

The deposition process for thin wall structures is illustrated in Fig. 2A. This type of structure was built using a reciprocating scan motion, where the laser head was incremented vertically after each layer by the layer height. Powder was fed using Powder Motion Labs X2W powder feeder, with a powder feed repeatability of <1%. Ceramic powders were conveyed to the melt pool with high-purity argon gas. Thin wall structures were fabricated using the parameters summarized in Table 1. It is worth noting that these optimized parameters were selected based on our recent studies of the effects of processing conditions on laser direct deposited ceramic part quality [18].

Cylindrical samples were printed to facilitate measurements of flexural strength and modulus on laser direct deposited alumina ceramics. This type of samples was prepared for each zirconia doping composition

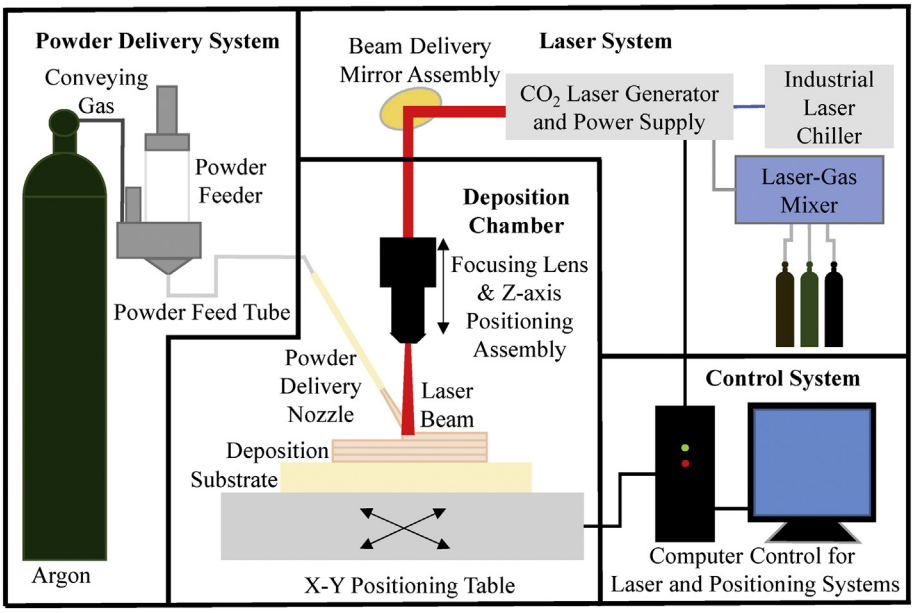

Fig. 1. A schematic of the laser direct deposition setup.

using the printing strategy illustrated in Fig. 2B. Cylinders were printed vertically from the substrate without movement in the x- or y-directions. The build rate in the z-direction was matched by feed rate of the laser head to ensure consistent and uniform deposition. The processing parameters used to deposit cylindrical structures are shown in Table 2. The printed cylindrical samples were approximately 60 mm in length, and the diameters ranged from 5 mm for pure alumina to 6 mm for 10 wt% zirconia content.

Thin wall structures fabricated with the aforementioned laser direct deposition process were sectioned using a low speed diamond saw and were then polished according to ASM standards [19]. To characterize the typical microstructure, the printed samples were sectioned near the middle section at a plane perpendicular to the scan direction, and parallel to the build direction. All samples were mounted in VariDur acrylic mounts prior to diamond saw sectioning to prevent post-processing induced damage to the samples. Pure alumina samples were thermally etched prior to taking images to aid in viewing grain boundaries. No thermal etching was used for samples with zirconia due to ease in viewing grain boundaries via zirconia placement.

The cross-sectional images of fabricated samples were taken using a Hirox KH-8700 digital microscope. FEI Quanta 600F and Hitachi S4700/EDAX were used for scanning electron microscopy (SEM) and energy

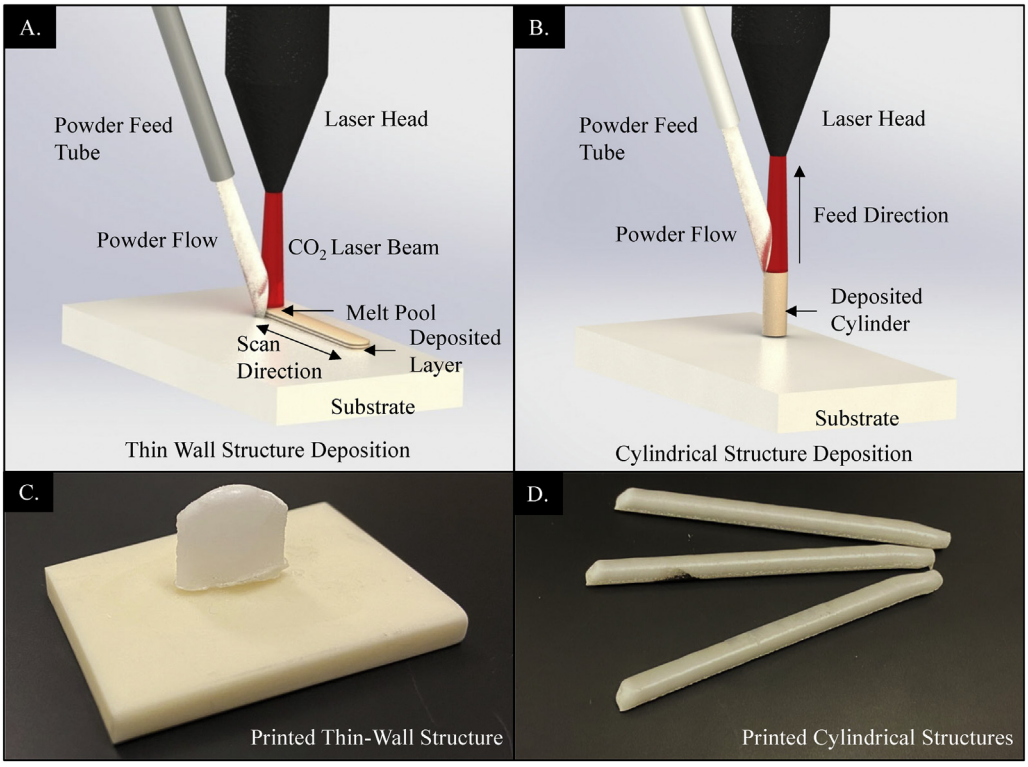

Fig. 2. Illustration of laser direct deposition processes for A. thin wall structures and B. cylindrical structures with typical printed parts shown in C and D, respectively.

Table 1
Process parameters for fabrication of thin wall structures.

Laser power (W)	275
Laser spot size (mm)	2.5
Scan speed (mm/min)	1000
Powder flow rate (g/min)	2.1

dispersive x-ray spectroscopy (EDS), respectively. Prior to SEM imaging, all alumina samples were sputter coated with gold-palladium coating with a thickness of 25 nm for better resolution. X-ray diffraction (XRD) analysis was performed on printed samples using a Philips X'Pert Pro multi-purpose diffractometer. Prior to analysis, samples were crushed to a fine powder. XRD peak analysis was done with X'pert HighScore software. Vickers microhardness measurements were taken on the cross-sections of polished thin wall structures printed with each zirconia doping composition. The results were averaged over ten indentations taken in the middle region of the cross-sections. A load of 9.8 N was applied to the sample surface and maintained for 10 s. Crack lengths originating from the diagonals of the Vickers indenter were measured using FIJI image processing software to calculate fracture toughness of printed samples. For purposes of fracture toughness calculations, elastic modulus was taken as 20*Hv (GPa) [7]. Flexural strength and modulus were determined using a four-point bending method on an Instron 5881 machine with a support span of 40 mm and a load span of 20 mm as shown in Fig. 3. Three samples of each composition were tested at a cross-head speed of 1 mm/min.

3. Results and discussion

3.1. Microstructural characterization

Fig. 4 shows fracture surfaces of thin wall (Fig. 4A–C) and cylindrical (Fig. 4D–F) samples prepared with doping compositions of 0 wt%, 5 wt%, and 10 wt% zirconia. Spherical pores were present for all three compositions, which were typically indicative of gas entrapment during the solidification process [20]. However, the frequency of pores was significantly less for the cylindrical samples compared to that of thin wall samples. The printing strategy used for cylindrical samples resulted in a continuous heat flux to recently deposited layers as the laser moved up in the z-direction. This resulted in more gradual cooling and allow more gasses to escape, leading to a reduction in porosity. On the other hand, for thin wall structures, the reciprocal printing path was characterized by large fluctuations in temperature at a given location during printing process. After material was deposited, the laser heating source quickly moved away from the location. This resulted in rapid cooling and solidification before gasses could escape to the surface of the melt pool. With increased laser heat input, as shown in our previous studies, the porosity of the thin wall samples would be greatly reduced, e.g., increasing laser power or controlling scan speed to allow more time for gasses to escape [21].

3.2. Grain size characterization

As shown in Fig. 4, the grain size of samples doped with zirconia was significantly smaller than that of pure alumina, showing that grain size control is possible through the addition of zirconia for laser direct deposited ceramics. The decreasing trend in grain size with respect to zirconia content was observed for both thin wall and cylindrical samples.

Table 2
Process parameters for fabrication of cylindrical structures.

Laser power (W)	275
Laser spot size (mm)	2.5
Feed rate (mm/min)	8
Powder flow rate (g/min)	2.1

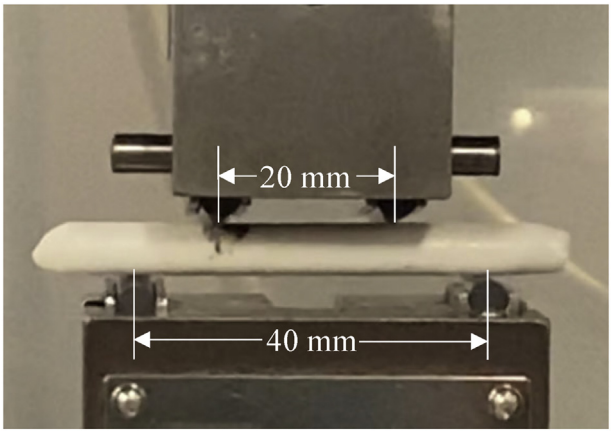

Fig. 3. Experimental setup for four-point bending test to measure flexural moduli and strength of the fabricated alumina ceramic samples.

Grain size within the thin wall samples was thus further characterized to quantify the noticeable differences observed between different zirconia doping percentages. Noticeable variations in grain size were also observed across the whole cross-section as shown in Fig. 5A, which was stitched from several optical microscope images in Fiji software using an image stitching plugin [22]. Four typical locations were thus chosen. Location **a** represents the top portion of the cross-section, where the final layers were deposited. Location **b** refers to the edge of the cross-section on the opposite side of incoming powder flow, near the middle of the sample. Location **c** is directly across from location **b** and is on the same side of incoming powder. Location **d** is in the central region of the cross-section, between **b** and **c**, but at a slightly lower position. These locations were chosen as they were indicative of the variations in cooling conditions throughout the samples during laser direct deposition process.

Grain size was characterized through equivalent circular area diameter [23]. Fig. 5B shows the average grain size measured at each specified location for pure alumina, 5 wt%, and 10 wt% zirconia doped ceramics. Pure alumina specimens at the location **d** showed the largest grain sizes with an average equivalent circular area over 100 μm. The samples doped with zirconia showed significantly decreased grain size at all four locations. At the location **d**, the average grain size of the samples containing 5 wt% zirconia was 23 μm, with the grain size of 10 wt% zirconia doped samples slightly smaller at an average of 18 μm. The significant reduction in grain size can be attributed to the fact that the introduced zirconia dopants reduced grain boundary mobility [24,25] and grain growth rate during solidification. Meanwhile, the relatively lower thermal conductivity due to zirconia dopants [26] decreased the size of laser heat affected zone and further lowered the possibility of grain growth within the previously deposited ceramic layers during printing process [27,28]. These combined led to the finer microstructure observed after doping alumina samples with zirconia.

An obvious variation in grain size was also observed across the same sample for each composition as seen in Fig. 5B. This result was typically observed in additively manufactured specimens, especially for directed energy deposition (DED) methods [29]. The variation in grain size was due to non-uniform solidification caused by differences in heating and cooling conditions across the samples. Boundary conditions imposed on the samples during deposition in this study included high laser energy input from the top, a continuous stream of cool argon gas and powder on one side, ambient temperature in the build chamber on the other side, and significant cooling through the substrate on the bottom. These combined led to highly diverse solidification characteristics within the same samples. It was also observed in Fig. 5B that the grain size

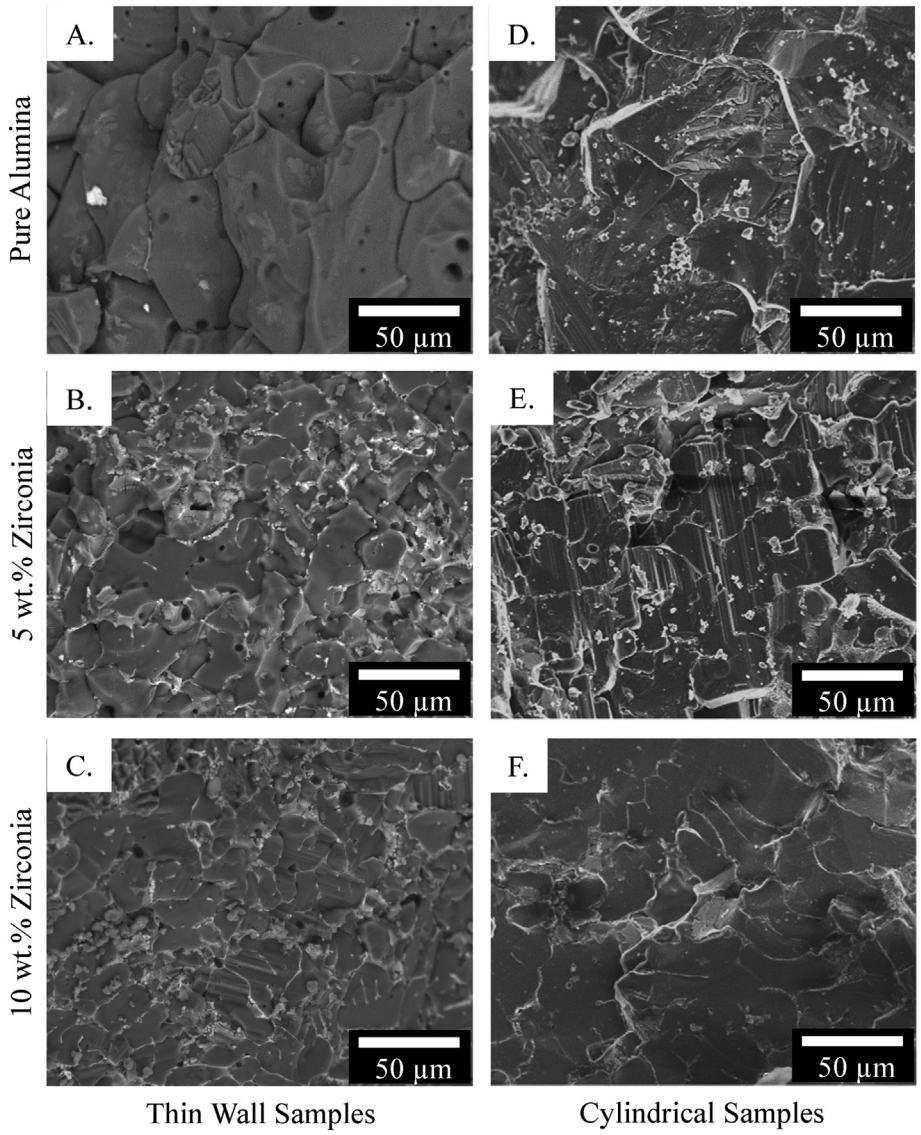

Fig. 4. SEM fractographs of thin wall samples printed with A. 0 wt%, B. 5 wt%, and C. 10 wt% zirconia, and fractographs of cylindrical samples printed with D. 0 wt%, E. 5 wt%, and F. 10 wt% zirconia.

variation was most pronounced in the pure alumina samples, with considerably less variation for the samples doped with 5 wt% and 10 wt% zirconia.

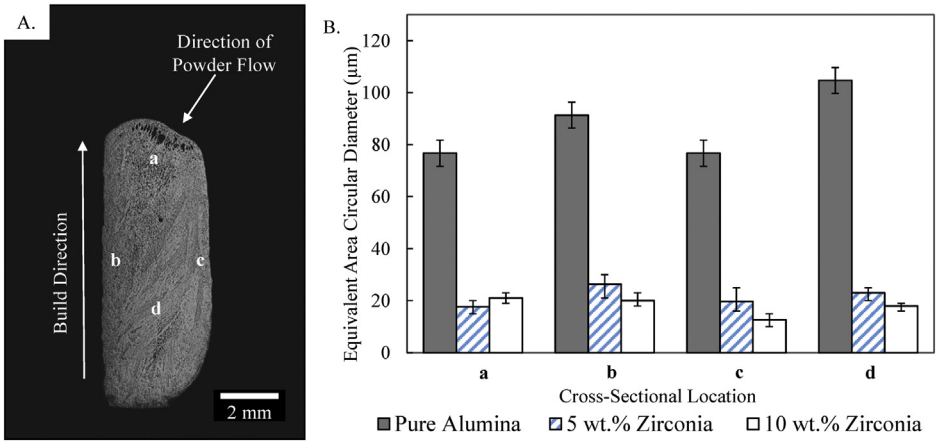

Fig. 5. A. Optical micrograph of the cross-sectional view of a typical 10 wt% zirconia sample showing the four locations chosen for microstructural characterization and B. Variation of grain size for each specified cross-sectional location with respect to zirconia percentage.

3.3. Composition characterization

A detailed X-ray diffraction (XRD) analysis was performed for as-received alumina and zirconia powders as well as all printed samples as shown in Fig. 6. Only α-alumina phase was detected consistently for the as-received alumina powders and all printed samples including pure, 5 wt% and 10 wt% zirconia doped alumina ceramics. Meanwhile, no obvious difference was observed for the doped zirconia before and after processing. In comparison of the as-received zirconia powders and the doped samples, both tetragonal and monoclinic zirconia phases were found with similar XRD patterns observed in Fig. 6.

The elemental composition for the thin wall samples doped with different zirconia was also characterized by EDS. Fig. 7 shows the SEM images with the corresponding EDS mapping for primary elemental constituents. As expected, the pure alumina sample showed only aluminum and oxygen. In contrast, the samples doped with zirconia not only showed aluminum and oxygen but also included zirconium, located exclusively along grain boundaries. During cooling and solidification, the zirconia phase precipitated out and segregated along alumina grain boundaries, forming the interface occupied by the added zirconia within laser melted and solidified alumina ceramics [30]. This effect was observed consistently across the fabricated alumina samples doped with both 5 wt% and 10 wt% zirconia.

Additional detailed investigation of the formed grain boundaries was performed. As shown in Fig. 8, both the 5 wt% and 10 wt% zirconia doped samples exhibited two distinct phases: a light phase along grain boundaries and a dark alumina phase. The elements of these two phases were analyzed with the locations of detection highlighted in Fig. 8. The location 1 showed the alumina phase in the grains while the location 2 showed the light phase along the grain boundaries. From the results summarized in Fig. 8C and Fig. 8D, a relatively consistent compositional distribution of primary elements was found in both the alumina phase and the light phase along grain boundaries. The added zirconium element was only found along the grain boundaries. Interestingly, aluminum was also detected within the light phase along the grain boundaries, possibly attributed to the formation of Al_2O_3-ZrO_2 eutectic colonies. A more obvious eutectic structure was observed in the highlighted region in Fig. 8D for the 10 wt% doped samples. Compared to the 5 wt% doped samples, a higher concentration of zirconia was found along the grain boundaries of the 10 wt% doped samples, thus increasing the possibility of the formation of eutectic structure. Meanwhile, the alumina phase exhibited an oxygen deficiency due to the formation of oxygen vacancies during melting, which was also recently found during deposition of yttria stabilized zirconia (YSZ) ceramics [15].

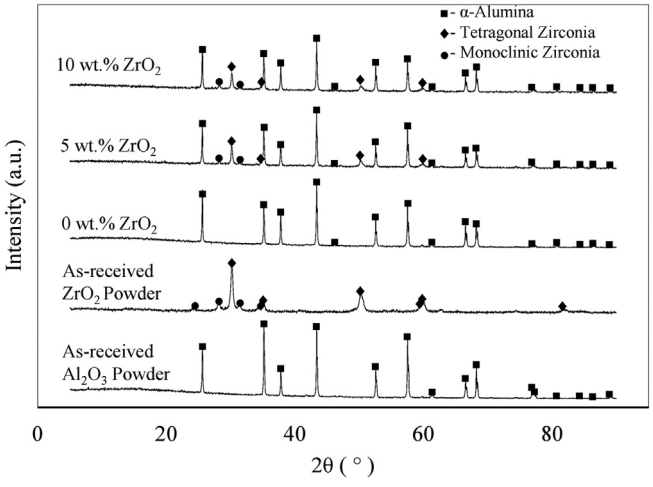

Fig. 6. XRD peak patterns for printed alumina samples doped with different percentages of zirconia. As-received alumina and zirconia powders are both characterized for comparison.

A post-annealing process is expected to restore the oxygen content and eliminate the vacancies.

3.4. Characterization of crack formation

A critical issue for brittle ceramics is their high tendency to form cracks due to very high cooling rates present during laser direct deposition process [10], which can be up to 10^5 K/s. High cooling rates induce internal stresses in the deposited part, and if the stresses are sufficiently high, crack initiation and propagation may occur. Internal cracks produced during fabrication are critical defects, severely limiting the mechanical strength of the fabricated samples. Traditional sintering methods typically use additives/dopants to densify and control the microstructure and properties. The addition of a second material could potentially induce interfacial crack-bridging and bifurcation mechanisms [2,6,31] and toughen the obtained ceramics. Thus, the effect of zirconia doping contents on the crack formation was explicitly investigated for the laser direct deposited alumina ceramics in this study.

Fig. 9 shows typical cross-sectional crack patterns for all three compositions fabricated at a laser power of 275 W and a scan speed of 1000 mm/min. For each composition in Fig. 9, the crack formation was further highlighted and used for crack length measurement. The primary types of cracks found in this study were microcracks that only propagated a short distance and were only visible at high magnifications, as well as macrocracks that were significantly longer and much more pronounced. Pure alumina specimens showed a high tendency to develop cracks distributed across the whole sample, which are clearly visible in Fig. 9A with a few typical macrocracks indicated by arrows. The cracks were typically transverse (along the horizontal direction) with crack bifurcation into the longitudinal (vertical) direction observed. In contrast, with the addition of zirconia, the occurrence of cracks was obviously reduced for the sample doped with 5 wt% zirconia as shown in Fig. 9B. After the zirconia was increased to 10 wt%, there were almost no noticeable cracks as shown in Fig. 9C.

The total crack length was measured and summarized in Fig. 10 for each composition. The number of cracks was also counted and used to calculate the average crack length as shown in Fig. 10. The total crack length for pure alumina was nearly 19 cm but was reduced by about 50% after adding 5 wt% zirconia. Only a total crack length of 0.15 cm (reduction by 99%) was observed after further increasing zirconia content to 10 wt%. The great reduction in crack formation could be attributed to the fact that the zirconia doping significantly refined the microstructure as seen above, which was expected to strengthen the deposited ceramics. In the meantime, the dopants that accumulated along the grain boundaries also helped toughen the alumina ceramics as further discussed below, thus making them less sensitive to thermal stresses during deposition through interfacial crack-bridging and bifurcation mechanisms [2,6,31]. These combined led to much fewer and shorter cracks observed here and showed the potentials as an alternative way to tailor the properties of laser direct deposited ceramics via dopants.

Interestingly, in comparison of pure alumina ceramics and the samples doped with 5 wt% zirconia, only a small variation in the average crack length was observed in Fig. 10. This is likely due to the relatively small amount of zirconia that was only sufficient to inhibit crack initialization but not crack propagation. In contrast, by further increasing zirconia contents to 10 wt%, not only was crack initiation hindered but crack propagation was likewise influenced. Further studies will be performed to examine the different cracking mechanisms exhibited due to zirconia doping during laser direct deposition process.

3.5. Porosity and density characterization

To study the doping effect on the densification of the printed samples, porosity, pore size distribution and density were investigated for all thin wall samples including pure, 5 wt% and 10 wt% zirconia doped alumina samples. Porosity measurements were taken on optical

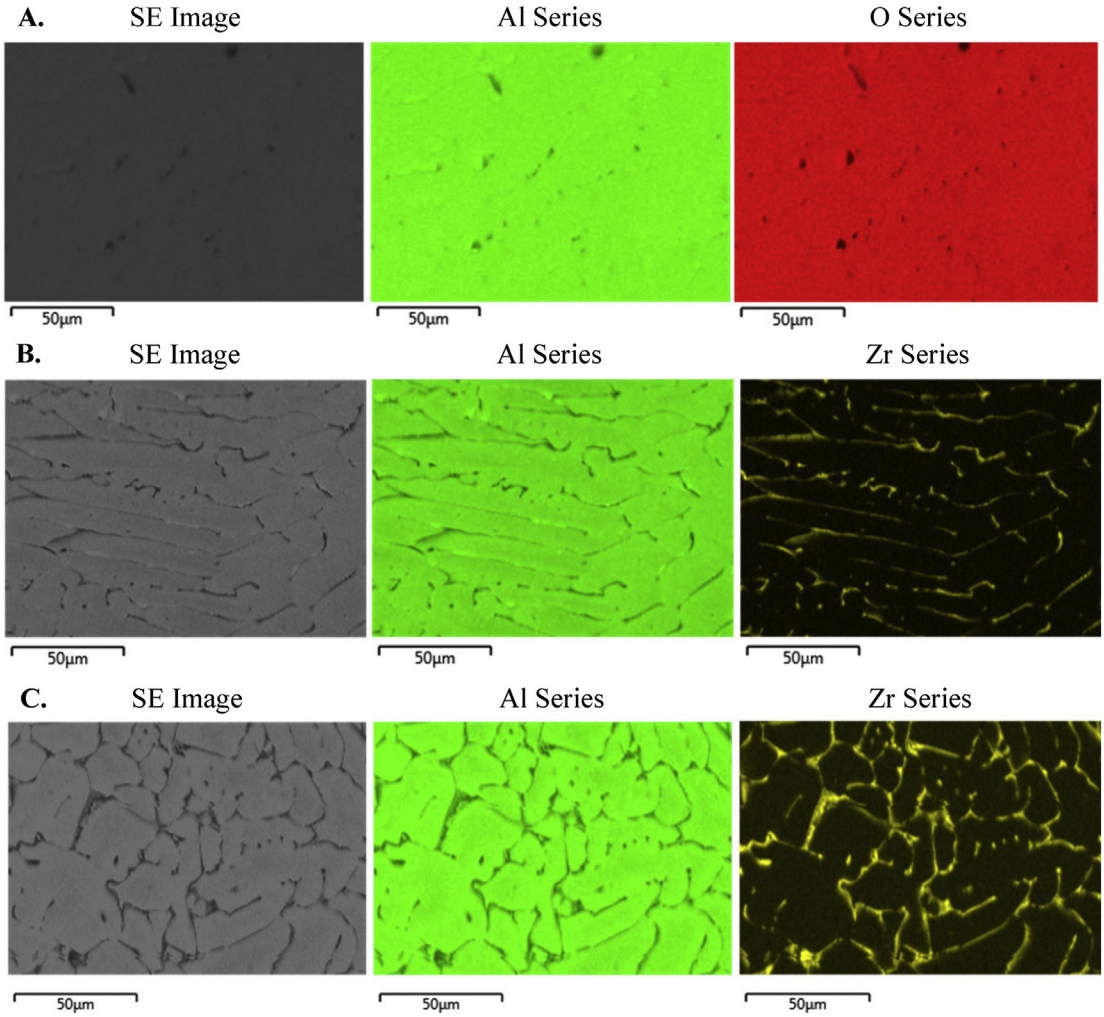

Fig. 7. Scanning electron micrographs and EDS elemental mapping illustrating the primary composition of alumina ceramics fabricated for A. Pure alumina, B. 5 wt% zirconia, and C. 10 wt% zirconia.

micrographs of the polished cross-sections of thin wall samples. The optical micrographs were first processed in Fiji image processing software by binarizing/thresholding to highlight pores as shown in Fig. 11. Pore area percentage was then measured using a particle analysis function. All printed samples showed gas porosity trapped during the deposition process.

The measured porosity in Fig. 12A increased with increasing zirconia doping percentages. The porosity change could be attributed to the different vapor pressures of alumina and zirconia during melting [32], resulting in inclusion of gas pores. Alumina has a much lower melting point (2135 °C) with its boiling point (2977 °C) [33] only about 260 °C lower than the melt point of zirconia (2715 °C). Under high irradiance during laser melting, vaporization of alumina is easily reached, creating additional gas bubbles within the melt before solidification and thus increasing porosity. This will also result in a higher concentration of zirconia in the final parts, in consistence with findings reported by Niu et al. [34] for eutectic alumina-zirconia ceramics. Meanwhile, the viscosity of the melt [35] is expected to be altered after the addition of zirconia and may contribute to increased porosity as well as different pore size distribution in Fig. 12B. A weighted histogram of pore size distribution is shown. The pore size was calculated by converting the measured area of individual pores into an equivalent circular diameter [23]. The histogram was normalized by the entire cross-sectional area analyzed. Hence, the height of each bar represented the area fraction of pores within the corresponding pore size range. Pure alumina samples exhibited a relatively uniform distribution of pore size ranging from approximately 1 μm up to above 30 μm. The addition of zirconia to alumina obviously increased the percentage of pores smaller than 25 μm. Further increasing zirconia to 10 wt% dramatically increased the percentage of pore size larger than 30 μm, mainly attributed to the formation of interconnected pores as seen in Fig. 11C with a decrease of smaller pores found in Fig. 12B. Further studies will also be performed to investigate the effect of dopants on the melt viscosity and its relationship with porosity during laser direct deposition of ceramics.

Density was determined via Archimedes' method. Relative density was calculated through dividing the measured density by the theoretical density of each sample. Here, the theoretical density values were taken as 3.97 g/cm^3 [36] and 6.05 g/cm^3 [37] for alumina and zirconia, respectively. The theoretical density for zirconia doped samples was calculated using the rule of mixtures [38]. The measured relative density in Fig. 13 decreased with an increase of zirconia doping percentage, attributed to the increased porosity seen in Fig. 12 after the addition of dopants.

3.6. Mechanical characterization

3.6.1. Microhardness

The effects of zirconia doping were also studied in terms of the mechanical properties of the additively manufactured alumina ceramics. The measured average microhardness (Hv) for alumina ceramics with each composition is shown in Fig. 14. Pure alumina showed the maximum hardness of all printed compositions with an average value of

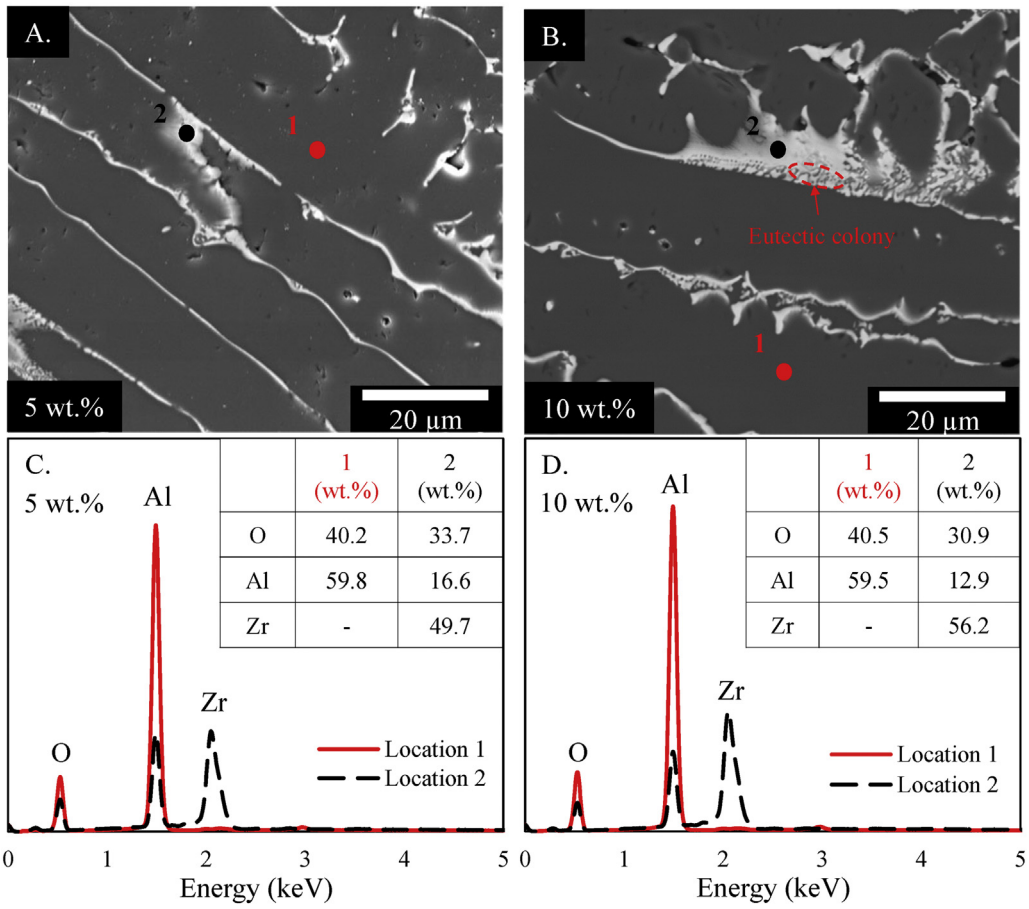

	1 (wt.%)	2 (wt.%)
O	40.2	33.7
Al	59.8	16.6
Zr	-	49.7

	1 (wt.%)	2 (wt.%)
O	40.5	30.9
Al	59.5	12.9
Zr	-	56.2

Fig. 8. SEM images of printed samples doped with A. 5 wt% and B. 10 wt% zirconia with C and D showing the elemental compositions of 5 wt% and 10 wt% samples, respectively. The locations 1 and 2 highlight the detected spots for grains and grain boundaries, respectively.

1880 Hv, comparable to the reported values obtained by traditional sintering methods [39]. With an increase of zirconia dopants, the measured average hardness values slightly decreased, reaching 1680 Hv for the samples doped with 10 wt% zirconia. It is worth noting that the decrease in hardness occurred despite the reduction in grain size observed above. It generally followed the declining trend predicted by the volumetric rule of mixtures (RoM) [40] as

$$Hc = f_{Al}H_{Al} + f_{Zr}H_{Zr} \quad (1)$$

where Hc denotes the hardness of the deposited alumina ceramics. f_{Al} and f_{Zr} are the volume fractions of alumina and zirconia, respectively. H_{Al} and H_{Zr} are the effective hardness of alumina phase and zirconia phase, respectively. The hardness of alumina was taken as 1850 Hv [39] and the hardness of zirconia was taken as 1350 Hv [41] for the RoM calculation here. By increasing the percentage of the softer zirconia phase, the overall predicted hardness of the composite decreased as seen in Fig. 14. As zirconia dopants further increase, the decreasing trend in hardness is expected to continue before reaching eutectic

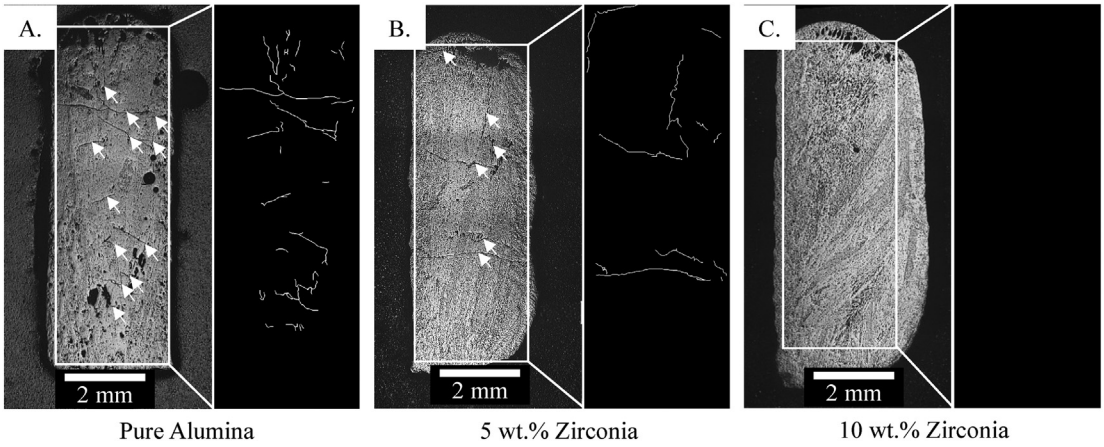

Fig. 9. Cross-sectional cracks (left) as highlighted for crack length analysis (right) within typical samples printed at a laser power of 275 W and a scan speed of 1000 mm/min: A. pure alumina, B. 5 wt% zirconia, and C. 10 wt% zirconia.

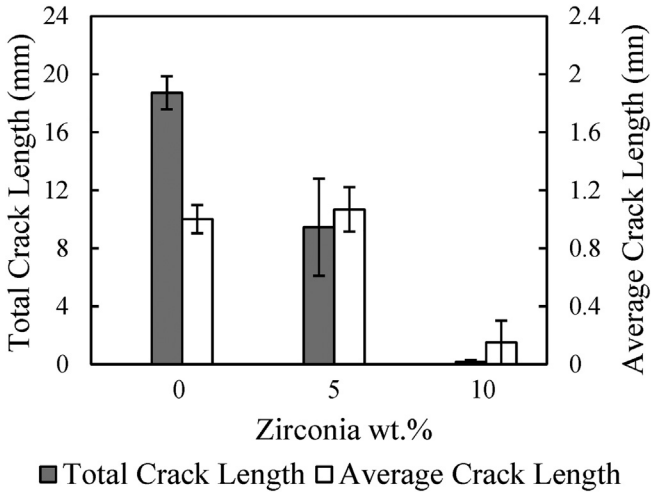

Fig. 10. Total and average crack length of samples printed with each zirconia doping composition.

ratio, where the microstructure was expected to be more significantly refined and may alter the trend [7].

In comparison to the predicted hardness values, the measured values decreased slightly more rapidly as shown in Fig. 14, particularly for the samples doped with 10 wt% zirconia, i.e., a measured value of 1680 Hv as opposed to a predicted value of 1835 Hv. This can be attributed to the fact that the predicted values were calculated based on the initial zirconia doping percentages, i.e., 5 wt% and 10 wt% in this study. However, the zirconia in the actual deposited samples may turn to be richer than initially doped percentages. Partially stabilized zirconia has a significantly higher melting point (2715 °C) compared to alumina (2072 °C). Thus, more evaporation of alumina during deposition potentially resulted in a higher concentration of zirconia in the final samples, as similarly observed by Niu et al. [34] during deposition of Al_2O_3-YAG eutectic ceramics. As the hardness of zirconia is lower than that of alumina, a concentration of zirconia could lower the effective hardness in comparison to the predicted values calculated based on the theoretical 5 wt% and 10 wt% in this study. Further studies will also be performed to study the composition change during laser direct deposition of alumina ceramics with dopants.

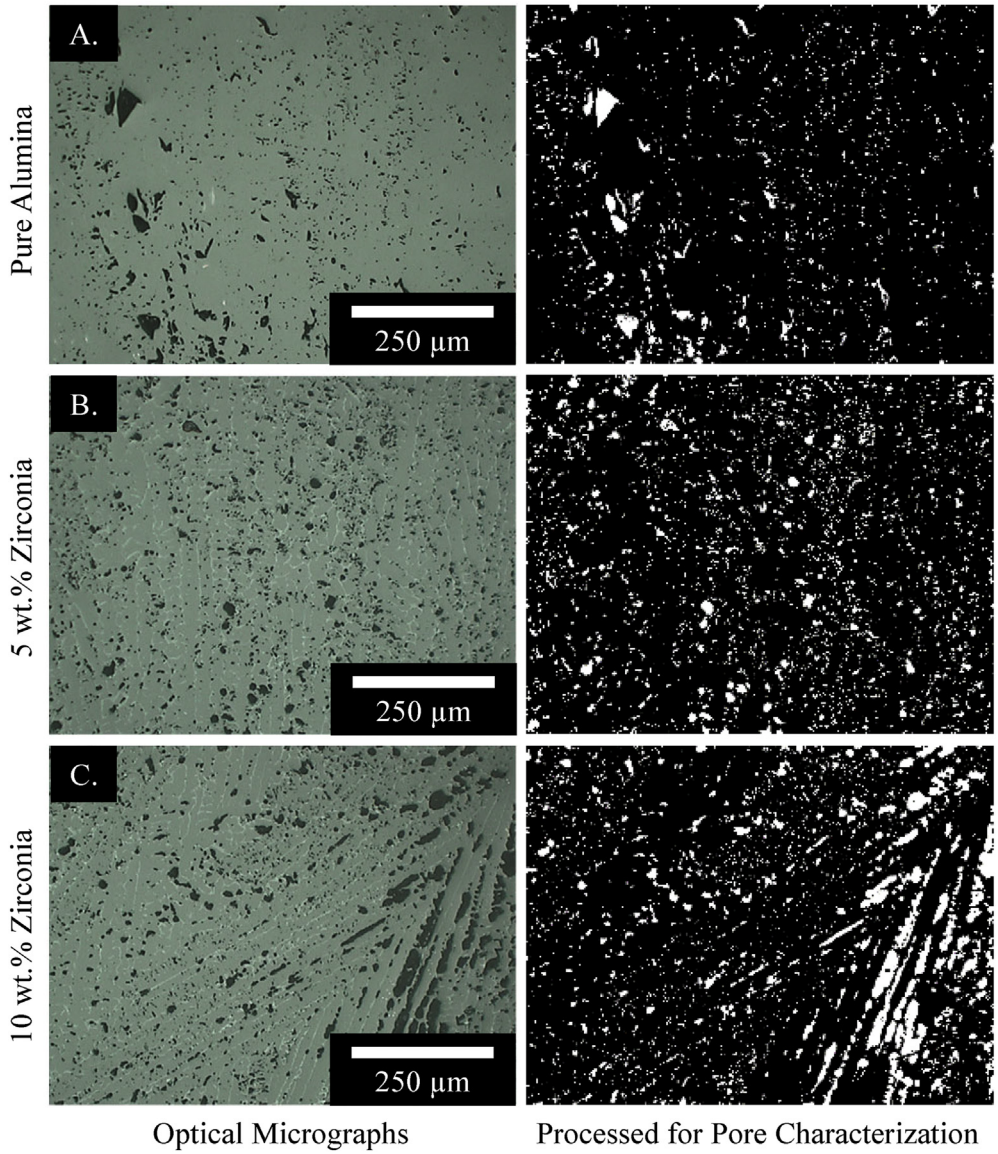

Fig. 11. Optical micrographs (left) and corresponding processed images for pore characterization (right) of A. pure alumina, B. 5 wt% zirconia and C. 10 wt% zirconia doped samples.

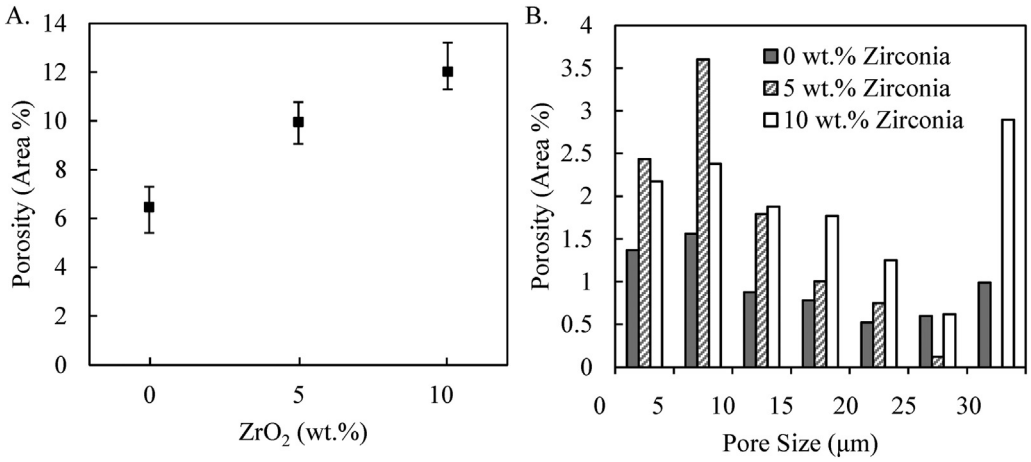

Fig. 12. Porosity analysis of samples printed at a laser power of 275 W and a scan speed of 1000 mm/min, where A. shows porosity area percentage measured at the middle region of the samples, and B. is a weighted histogram showing pore size distribution.

3.6.2. Fracture toughness

As suggested from the characterization of crack formation above, the doped zirconia potentially toughened the alumina grain boundary and thus exhibited significantly fewer and shorted cracks observed. The fracture toughness of the fabricated samples with different compositions was thus measured. As shown in Fig. 15, the length (l) of palmqvist cracks induced by Vickers indentation on the polished surface of thin wall samples was first measured for each zirconia doping composition. The fracture toughness (K_{IC}) was then calculated by [42]

$$\left(\frac{K_{IC}\cdot\varnothing}{Ha^{1/2}}\right)\cdot\left(\frac{H}{E\cdot\varnothing}\right)^{\frac{2}{5}} = 0.035\cdot\left(\frac{l}{a}\right)^{-3/2} \quad (2)$$

where H is the hardness. $\varnothing \cong 3$ is a constant. E is Young's modulus, approximated as $E \cong 20 \cdot H$ [7]. a denotes the indent half diagonal. It is worth noting the dark phase with nearly circular shape corresponded to the pores observed in the fabricated thin wall samples in Fig. 11.

As shown in Fig. 16, the measured fracture toughness greatly increased after adding the zirconia as dopants, indicating obvious toughening effects on the fabricated alumina samples. The fabricated pure alumina samples exhibited a value of 2.6 MPa*m$^{1/2}$. It increased to 3.8 MPa*m$^{1/2}$ (by about 46%) after adding 5 wt% zirconia. A similar trend was also observed for laser deposited alumina/aluminum titanate composites [7]. The increase in fracture toughness was attributed to the zirconia dopants that accumulated along alumina grain boundaries, which interacted with crack formation and promoted crack deflection, crack bifurcation, and crack pinning, as typically observed in Fig. 15B and Fig. 15C for the samples doped with 5 wt% and 10 wt% zirconia, respectively. Crack deflection and bifurcation consumed much of fracture energy during crack formation and thus toughened the ceramics. In contrast, these toughening mechanisms were primarily absent for the pure alumina sample with crack deflection observed in Fig. 15A. Besides the crack interaction with the zirconia doped grain boundary, a stress induced phase change of tetragonal zirconia (as detected above in the printed samples) into the monoclinic crystal structure was also found in previous studies [5], leading to a volume expansion of 3–5% and shear strain of approximately 7%. The compressive stresses induced by the volume expansion consumed more fracture energy and resulted in the observed toughening effect. These also helped explain the significantly reduced crack formation after adding dopants in the fabricated alumina samples as discussed above.

It is also worth noting that with a further increase in zirconia to 10 wt%, the fracture toughness slightly decreased to 3.4 MPa*m$^{1/2}$ in comparison to that of 5 wt% dopants. An initial increase followed by a decrease in fracture toughness was commonly observed in traditionally sintered alumina-zirconia ceramics [5,6,43]. A similar toughening mechanism was also expected to exist for the laser direct deposited

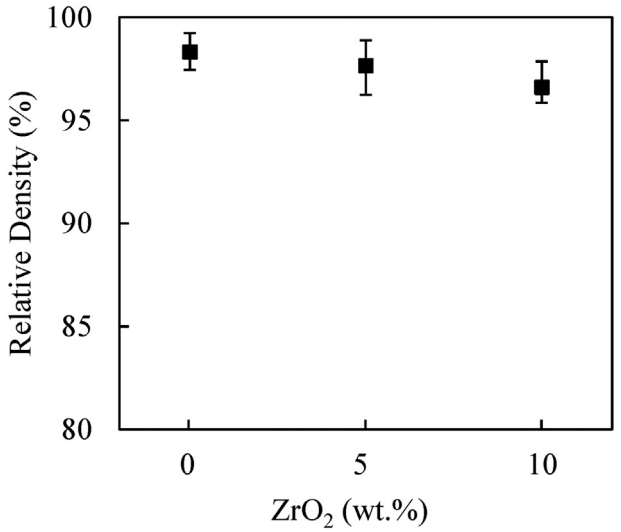

Fig. 13. Relative density of printed samples at each zirconia doping percentage.

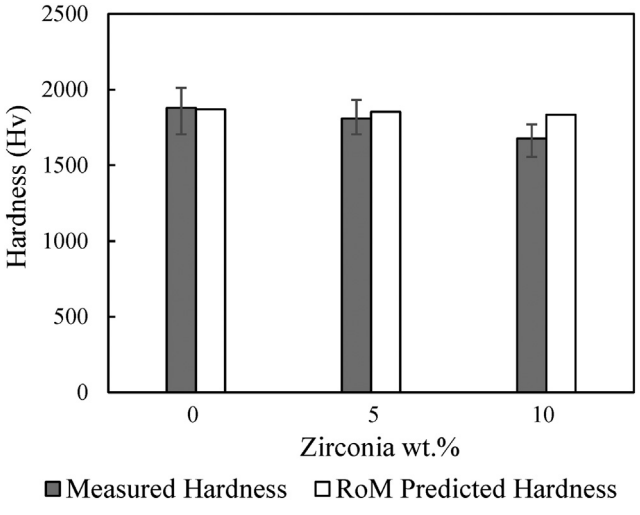

Fig. 14. Effect of zirconia doping on hardness of each composition in comparison to the hardness values predicted by the volumetric rule of mixtures.

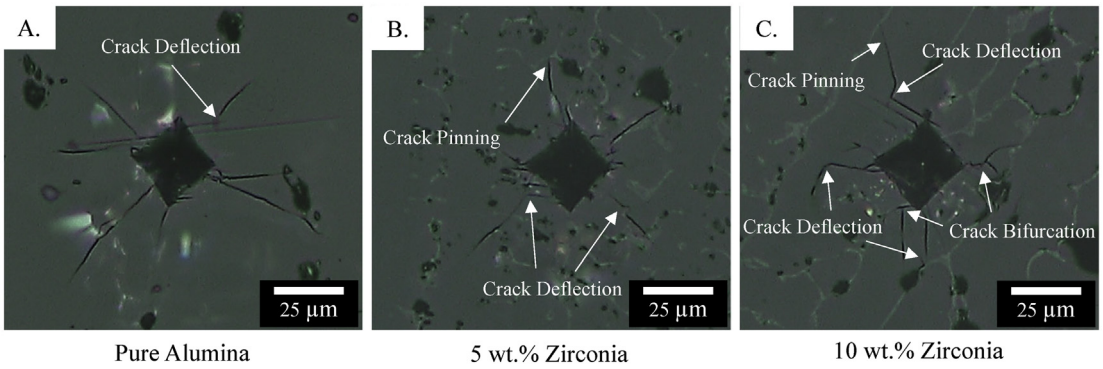

Fig. 15. Typical indentation crack patterns for A. Pure alumina, B. 5 wt% zirconia, and C. 10 wt% zirconia.

alumina ceramics here. The benefits of zirconia addition on toughness are limited by the amount of zirconia present in the fabricated samples. If too much zirconia is present, the ratio of monoclinic to tetragonal zirconia increases and will limit phase transformation toughening effects [6], resulting in slightly lower toughness values. Therefore, it is necessary to design zirconia doping and further tailor the fracture toughness of additively manufactured ceramics via laser direct deposition. It is also worth noting that although yttria (3 mol%) was added in the initial powder to partially stabilize tetragonal zirconia [44], further studies will be needed to evaluate its effect on the final alumina samples after going through the full melting and solidification cycles during deposition process.

3.6.3. Flexural modulus and strength

The flexural moduli and strength of the deposited cylindrical alumina samples were also measured through four-point bending tests discussed above. The measured values for each doping composition are summarized in Fig. 17. The flexural modulus decreased dramatically with the addition of zirconia, from approximately 150 GPa for pure alumina down to 32 GPa for the 10 wt% zirconia doped samples. As the modulus of alumina phase (370 GPa [45]) was much larger than that of partially stabilized zirconia phase (210 GPa [46]), increasing the percentage of softer zirconia dopants would decrease the effective modulus of the alumina samples. In contrast, with an increase in zirconia percentage, a substantial increase in flexural strength was observed, from an average value of 58 MPa for the pure alumina samples to 208 MPa for the samples doped with 10 wt% zirconia.

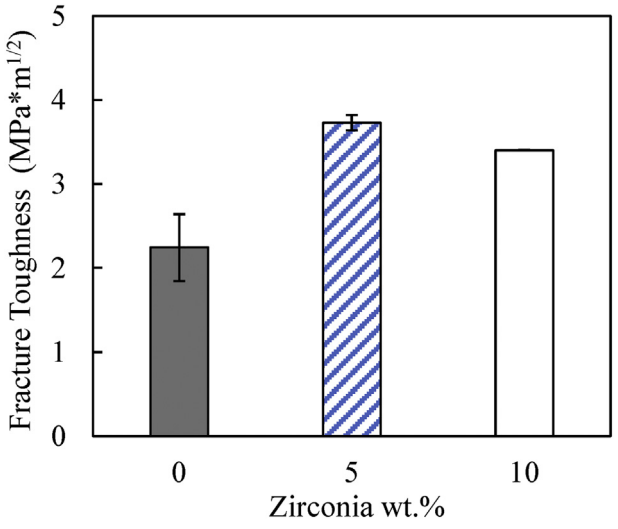

Fig. 16. Effect of ZrO_2 doping contents on the fracture toughness of the fabricated alumina samples.

It is worth noting that the measured flexural modulus and strength of the laser direct deposited alumina ceramics were much lower than those reported for the traditionally sintered alumina ceramics [45,46]. The primary factor contributing to the large difference was the critical flaw size present within the deposited alumina samples, often related to the defects formed during the deposition process, e.g., residual pores and cracks. Thus, the critical flaw size (C) of the fabricated samples was further approximated by Griffith criterion to characterize the defects within the deposited alumina samples as

$$C = \frac{{K_{IC}}^2}{\pi \cdot {\sigma_f}^2} \tag{3}$$

where K_{IC} is the fracture toughness and σ_f is the flexural strength. The values of fracture toughness, flexural strength, and the calculated critical flaw size are summarized in Table 3. The critical flaw size for pure alumina was largest, corresponding to the lowest flexural strength observed among all three different compositions. Meanwhile, the obtained critical flaw size for 10 wt% zirconia doped samples was significantly lower than those of both pure alumina samples and 5 wt% zirconia doped samples. The trend here correlated well with the findings for crack formation seen in Fig. 10, where the deposited pure alumina samples showed largest crack length, and the average crack length of both pure alumina samples and 5 wt% zirconia samples was greatly higher than that of 10 wt% zirconia samples. These cracks, as one critical defect formed during deposition process and captured as the critical flaw size here, would act as pre-existing defects during bending tests. The increase of pre-existing cracks would severely limit the ceramics ability to withstand tensile stresses generated under bending tests, leading to the brittle failure of the samples at much lower loads [47] as

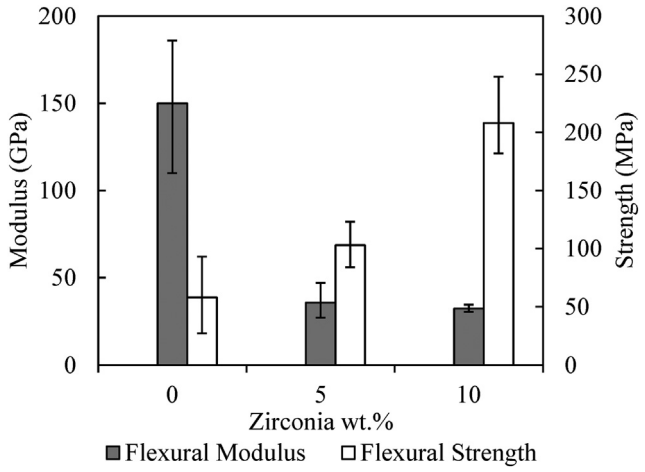

Fig. 17. Effect of ZrO_2 doping contents on flexural modulus and strength.

Table 3
Critical flaw size for each composition determined by Griffith fracture criterion.

Material	K_{IC} (MPa*m$^{1/2}$)	Flexural strength (MPa)	Critical flaw size (μm)
Pure alumina	2.6	58	660
5 wt% zirconia	3.8	103	440
10 wt% zirconia	3.4	208	85

demonstrated by the lower flexural strength measured in Table 3. It is also worth noting that while further studies are still needed to further understand the mechanisms of defect formation, the addition of zirconia dopants was shown as one efficient way of reducing the defects, particularly crack formation, which is one critical issue during laser direct deposition of brittle ceramic materials.

The significant reduction in critical flaw size observed for larger zirconia doping contents could be attributed to the grain refinement observed in Fig. 4. For the cylindrical samples, the 10 wt% zirconia doped composition exhibited the smallest grain size. Through grain refinement and thus reduction in critical flaw size, zirconia greatly improved the flexural strength of the deposited ceramics [48]. The results also well demonstrated that zirconia doping helped tailor the microstructure and resultant mechanical properties of laser direct deposited ceramics.

4. Conclusions

This study investigated the effects of zirconia dopants on laser direct deposited alumina ceramics. Significant grain refinement was achieved by adding low amounts of zirconia. Average grain sizes were 100 μm, 23 μm, and 18 μm for pure alumina, 5 wt%, and 10 wt% zirconia doped samples, respectively. Grain size was primarily affected by decreased grain boundary mobility and thermal conductivity with increased zirconia doping amounts. Addition of zirconia also reduced the prevalence of cracking compared to pure alumina samples. Crack prevalence was highly dependent on zirconia content, where the samples doped with 10 wt% zirconia were nearly crack-free. The zirconia dopants, which accumulated along alumina grain boundaries as confirmed by detailed composition analysis, interacted with crack formation and helped toughen the bulk structures through the tetragonal to monoclinic transformation within the printed samples. Meanwhile, the addition of zirconia dopants increased porosity and altered pore size distribution. Grain refinement obtained by increasing zirconia content, accompanied by greatly reduced critical flaw size, was shown to substantially improve flexure strength from 58 MPa for the pure alumina samples to 208 MPa for the samples printed with 10 wt% zirconia. Added zirconia was also shown to improve fracture toughness substantially, with the highest K_{IC} values recorded for a zirconia dopant content of 5 wt%. This study showed that zirconia dopants can be used to tailor microstructure and mechanical properties of additively manufactured alumina ceramic samples. The insights gained provided further opportunities in designing ceramic components fabricated by laser direct deposition via doping to meet the specific requirements for a variety of applications.

CRediT authorship contribution statement

John M. Pappas: Conceptualization, Methodology, Investigation, Data curation, Writing - original draft. **Aditya R. Thakur:** Methodology, Investigation. **Xiangyang Dong:** Supervision, Project administration, Funding acquisition, Writing - review & editing.

Declaration of competing interest

The authors declare that they have no known competing financial interests or personal relationships that could have appeared to influence the work reported in this paper.

Acknowledgements

The authors would like to thank Dr. Jeremy Watts, at Missouri S&T for sharing his expertise and aid in sample preparation for microstructural analysis. They would also like to thank Joe Atria at Almatis for generously supplying the alumina powder used in this research. A special thanks would be extended to Dr. Eric Bohannan at the Materials Research Center of Missouri S&T for his expertise and assistance with X-ray diffraction experiments and analysis. The authors acknowledge the funding support provided by US Department of Education Grant P200A180061 in part of John M. Pappas's research work.

References

[1] F.A. Al-Sanabani, A.A. Madfa, N.H. Al-Qudaimi, Alumina ceramic for dental applications: a review article, Am. J. Mater. Res. Am. J. Mater. Res. Am. J. Mater. Res. Am. J. Mater. Res. 1 (2014) 26–34.
[2] Y. Hu, F. Ning, W. Cong, Y. Li, X. Wang, H. Wang, Ultrasonic vibration-assisted laser engineering net shaping of ZrO2-Al2O3 bulk parts: effects on crack suppression, microstructure, and mechanical properties, Ceram. Int. 44 (2018) 2752–2760, https://doi.org/10.1016/j.ceramint.2017.11.013.
[3] R. Danzer, A general strength distribution function for brittle materials, J. Eur. Ceram. Soc. 10 (1992) 461–472, https://doi.org/10.1016/0955-2219(92)90021-5.
[4] F. Kern, Microstructure and mechanical properties of hot-pressed alumina - 5 vol% zirconia nanocomposites, J. Ceram. Sci. Technol. 2 (2011) 69–74, https://doi.org/10.4416/JCST2010-00038.
[5] A.H. De Aza, J. Chevalier, G. Fantozzi, M. Schehl, R. Torrecillas, Crack growth resistance of zirconia toughened alumina ceramics for joint prostheses, Key Eng. Mater. 23 (2001) 1535–1538, https://doi.org/10.4028/www.scientific.net/kem.206-213.1535.
[6] V. Naglieri, P. Palmero, L. Montanaro, J. Chevalier, Elaboration of alumina-zirconia composites: role of the zirconia content on the microstructure and mechanical properties, Materials (Basel) 6 (2013) 2090–2102, https://doi.org/10.3390/ma6052090.
[7] D. Wu, Y. Huang, F. Niu, G. Ma, S. Yan, C. Li, J. Ding, Effects of TiO2 doping on microstructure and properties of directed laser deposition alumina/aluminum titanate composites, Virtual Phys. Prototyp. 14 (2019) 371–381, https://doi.org/10.1080/17452759.2019.1622987.
[8] J. Wilkes, Y.C. Hagedorn, W. Meiners, K. Wissenbach, Additive manufacturing of ZrO2-Al2O3ceramic components by selective laser melting, Rapid Prototyp. J. 19 (2013) 51–57, https://doi.org/10.1108/13552541311292736.
[9] F. Li, Y. Zhang, Microstructural characterization of Al 2 O 3 -ZrO 2 ceramic by laser direct material deposition, J. Laser Appl. 31 (2019), 022509. https://doi.org/10.2351/1.5096125.
[10] V.K. Balla, S. Bose, A. Bandyopadhyay, Processing of bulk alumina ceramics using laser engineered net shaping, Int. J. Appl. Ceram. Technol. 5 (2008) 234–242, https://doi.org/10.1111/j.1744-7402.2008.02202.x.
[11] F. Niu, D. Wu, F. Lu, G. Liu, G. Ma, Z. Jia, Microstructure and macro properties of Al2O3 ceramics prepared by laser engineered net shaping, Ceram. Int. 44 (2018) 14303–14310, https://doi.org/10.1016/j.ceramint.2018.05.036.
[12] F. Niu, D. Wu, G. Ma, J. Wang, M. Guo, B. Zhang, Nanosized microstructure of Al2O3-ZrO2 (Y2O3) eutectics fabricated by laser engineered net shaping, Scr. Mater. 95 (2015) 39–41, https://doi.org/10.1016/j.scriptamat.2014.09.026.
[13] S. Yan, D. Wu, F. Niu, Y. Huang, N. Liu, G. Ma, Effect of ultrasonic power on forming quality of nano-sized Al 2 O 3 -ZrO 2 eutectic ceramic via laser engineered net shaping (LENS), Ceram. Int. 44 (2018) 1120–1126, https://doi.org/10.1016/j.ceramint.2017.10.067.
[14] G.T.M. Stam, E. van der Giessen, P. Meijers, Effect of transformation-induced shear strains on crack growth in zirconia-containing ceramics, Int. J. Solids Struct. 31 (1994) 1923–1948, https://doi.org/10.1016/0020-7683(94)90200-3.
[15] Z. Fan, Y. Zhao, M. Lu, H. Huang, Yttria stabilized zirconia (YSZ) thin wall structures fabricated using laser engineered net shaping (LENS), Int. J. Adv. Manuf. Technol. (2019)https://doi.org/10.1007/s00170-019-03322-z.
[16] S.K. Makhija, N.C. Lawson, G.H. Gilbert, M.S. Litaker, J.A. Mcclelland, D.R. Louis, V. Valeria, D.J. Pihlstrom, C. Meyerowitz, Dentist material selection for single-unit crowns: findings from the National Dental Practice-Based Research Network, J. Dent. (2017) 40–47, https://doi.org/10.1016/j.jdent.2016.09.010.Dentist.
[17] J.H. Ouyang, S. Nowotny, A. Richter, E. Beyer, Laser cladding of yttria partially stabilized ZrO2 (YPSZ) ceramic coatings on aluminum alloys, Ceram. Int. (2001)https://doi.org/10.1016/S0272-8842(00)00036-5.
[18] J.M. Pappas, X. Dong, Effects of processing conditions on laser direct deposited alumina ceramics, ASME Manuf. Sci. Eng. Conf, American Society of Mechanical Engineers, Cincinnati, Ohio, USA, 2020.

[19] U. Ta, V. Carle, U. Scha, M.J. Hoffmann, Preparation and microstructural analysis of high-performance ceramics, Metallogr. Microstruct. 9 (2018) 1057–1066, https://doi.org/10.31399/asm.hb.v09.a0003795.
[20] P.A. Kobryn, E.H. Moore, S.L. Semiatin, Effect of laser power and traverse speed on microstructure, porosity, and build height in laser-deposited Ti-6Al-4V, Scr. Mater. 43 (2000) 299–305, https://doi.org/10.1016/S1359-6462(00)00408-5.
[21] J.M. Pappas, X. Dong, Porosity characterization of additively manufactured transparent MgAl2O4 spinel by laser direct deposition, Ceram. Int. 46 (2020) 6745–6755, https://doi.org/10.1016/j.ceramint.2019.11.164.
[22] S. Preibisch, S. Saalfeld, P. Tomancak, Globally optimal stitching of tiled 3D microscopic image acquisitions, Bioinformatics 25 (2009) 1463–1465, https://doi.org/10.1093/bioinformatics/btp184.
[23] M. Li, D. Wilkinson, K. Patchigolla, Comparison of particle size distributions measured using different techniques, Part. Sci. Technol. 23 (2005) 265–284, https://doi.org/10.1080/02726350590955912.
[24] R. Akiva, A. Katsman, W.D. Kaplan, Anisotropic grain boundary mobility in undoped and doped alumina, J. Am. Ceram. Soc. 97 (2014) 1610–1618, https://doi.org/10.1111/jace.12787.
[25] M.M. Gong, C.H. Chang, L.J. Wu, S. Dey, R.H.R. Castro, F. Liu, Modeling the grain growth kinetics of doped nearly fully dense nanocrystalline ceramics, Ceram. Int. 43 (2017) 6677–6683, https://doi.org/10.1016/j.ceramint.2017.02.062.
[26] N.P. Bansal, D. Zhu, Thermal conductivity of zirconia-alumina composites, Ceram. Int. 31 (2005) 911–916, https://doi.org/10.1016/j.ceramint.2004.09.018.
[27] T.M. Rodgers, J.E. Bishop, J.D. Madison, Direct numerical simulation of mechanical response in synthetic additively manufactured microstructures, Model. Simul. Mater. Sci. Eng. 26 (2018), 55010. https://doi.org/10.1088/1361-651x/aac616.
[28] T.M. Rodgers, J.A. Mitchell, V. Tikare, A Monte Carlo model for 3D grain evolution during welding, Model. Simul. Mater. Sci. Eng. 25 (2017), 64006. https://doi.org/10.1088/1361-651x/aa7f20.
[29] W.J. Sames, F.A. List, S. Pannala, R.R. Dehoff, S.S. Babu, The metallurgy and processing science of metal additive manufacturing, Int. Mater. Rev. 61 (2016) 315–360, https://doi.org/10.1080/09506608.2015.1116649.
[30] P. Ctibor, P. Rohan, T. Chraska, K. Neufuss, Fabrication of bulk nanocrystalline alumina – zirconia materials, 34 (2008) 1229–1236, https://doi.org/10.1016/j.ceramint.2007.04.001.
[31] Z. Liu, K. Song, B. Gao, T. Tian, H. Yang, X. Lin, W. Huang, Microstructure and mechanical properties of Al2O3/ZrO2 directionally solidified eutectic ceramic prepared by laser 3D printing, J. Mater. Sci. Technol. 32 (2016) 320–325, https://doi.org/10.1016/j.jmst.2015.11.017.
[32] N. Sakamoto, S. Araki, M. Yoshimura, Fabrication of nanocomposite ceramics by crystallization of rapidly solidified eutectic melts, J. Am. Ceram. Soc. 92 (2009) S157–S161, https://doi.org/10.1111/j.1551-2916.2008.02741.x.
[33] D. Schmidtmeier, G. Büchel, A. Buhr, Magnesium aluminate spinel raw materials for high performance refractories for steel ladles, Ceram. Mater. 61 (2009) 223–227.
[34] D. Wu, J. Wang, G. Ma, Z. Jin, F. Niu, J. Zhuang, Rapid fabrication of eutectic ceramic structures by laser engineered net shaping, Procedia CIRP 42 (2016) 91–95, https://doi.org/10.1016/j.procir.2016.02.196.
[35] Q. Chen, G. Guillemot, C.-A. Gandin, M. Bellet, Three-dimensional finite element thermomechanical modeling of additive manufacturing by selective laser melting for ceramic materials, Addit. Manuf. 16 (2017) 124–137, https://doi.org/10.1016/j.addma.2017.02.005.
[36] International Labor Organization, Aluminium Oxide, 2000.
[37] Tosoh, Advanced Ceramics |Zirconia Powders – High Translucent Grades, 2019.
[38] B. Agarwal, L. Broutman, K. Chandrashekhara, Analysis and Performance of Fiber Composites, Third John Wiley & Sons, Ltd, 2015.
[39] P. Figiel, M. Rozmus, B. Smuk, Properties of alumina ceramics obtained by conventional and non-conventional methods for sintering ceramics, J. Achiev. Mater. Manuf. Eng. 48 (2011) 29–34.
[40] H.S. Kim, On the rule of mixtures for the hardness of particle reinforced composites, Mater. Sci. Eng. A 289 (2000) 30–33, https://doi.org/10.1016/S0921-5093(00)00909-6.
[41] A. Miriyev, S. Grützner, L. Krüger, S. Kalabukhov, N. Frage, Bonding of TRIP-steel/Al2O3-(3Y)-TZP composites and (3Y)-TZP ceramic by a spark plasma sintering (SPS) apparatus, Materials (Basel) 9 (2016)https://doi.org/10.3390/MA9070558.
[42] K. Niihara, A fracture mechanics analysis of indentation-induced Palmqvist crack in ceramics, J. Mater. Sci. Lett. 2 (1983) 221–223, https://doi.org/10.1007/BF00725625.
[43] D.J. GREEN, Critical microstructures for microcracking in Al2O3-ZrO2 composites, J. Am. Ceram. Soc. 65 (1982) 610–614, https://doi.org/10.1111/j.1151-2916.1982.tb09939.x.
[44] S.M. Kurtz, S. Kocagöz, C. Arnholt, R. Huet, M. Ueno, W.L. Walter, Advances in zirconia toughened alumina biomaterials for total joint replacement, J. Mech. Behav. Biomed. Mater. 31 (2014) 107–116, https://doi.org/10.1016/j.jmbbm.2013.03.022.
[45] CoorsTek, Advanced alumina materials data sheet, Shock (2015) 1–2.
[46] CoorsTek, Advanced Zirconias for Severe-Service Environments, https://www.coorstek.com/media/4256/zirconia-materials.pdf 2017. (Accessed 12 January 2020).
[47] D. Askeland, W. Wright, The Science and Engineering of Materials, Seventh Global Engineering, 2014.
[48] R.M. Spriggs, T. Vasilos, Effect of grain size on transverse bend strength of alumina and magnesia, J. Am. Ceram. Soc. 46 (1961) 224–228.